Nuclear Instruments and Methods in Physics Research A 737 (2014) 22–28

Contents lists available at ScienceDirect

Nuclear Instruments and Methods in Physics Research A

journal homepage: www.elsevier.com/locate/nima

A digital data acquisition framework for the Versatile Array of Neutron Detectors at Low Energy (VANDLE)

S.V. Paulauskas [a,*], M. Madurga [a], R. Grzywacz [a,b], D. Miller [a], S. Padgett [a], H. Tan [c]

[a] The University of Tennessee at Knoxville, Department of Physics & Astronomy, Knoxville, TN 37996-1200, USA
[b] Oak Ridge National Laboratory, Oak Ridge, TN 37831, USA
[c] XIA LLC, 31057 Genstar Road, Hayward, CA 94544, USA

ARTICLE INFO

Article history:
Received 11 September 2013
Received in revised form
5 November 2013
Accepted 7 November 2013
Available online 20 November 2013

Keywords:
Plastic scintillators
Timing
Digitizers
Time-of-flight
Neutron detection

ABSTRACT

Neutron energy measurements can be achieved using time-of-flight (ToF) techniques. A digital data acquisition system was developed for reliable ToF measurements with subnanosecond timing resolution based on digitizers with 10 ns and 4 ns sampling periods using pulse shape analysis algorithms. A validation procedure was developed to confirm the reliability. The response of the algorithm to photomultiplier signals was studied using a specially designed experimental system based on fast plastic scintillators. The presented developments enabled digital data acquisition systems to instrument the recently developed Versatile Array of Neutron Detectors at Low-Energy (VANDLE).

1. Introduction

In this work, we present critical development steps for the Versatile Array of Neutron Detectors at Low Energy (VANDLE) [1,2]. These steps include the implementation and characterization of timing algorithms and a new triggering model. These developments enable VANDLE to be fully instrumented with a digital data acquisition system. Digital data acquisition systems are rapidly becoming common in nuclear physics experiments due to their many advantages with respect to analog electronics [3,4]. The main feature of such systems is a reliance on numerical algorithms that operate on digitized representations of the electrical pulse from a detector. The flexibility offered by an unlimited choice of pulse shape analysis methods is one reason for the growing demand of these systems.

However, an important limitation of this approach is the finite amplitude and time resolution of the analog to digital converters (ADCs) used to digitize the signals from the detectors. As a result, the digital image of the signal is a distorted version of the "real" signal. This distortion comes from the frequency cutoffs imposed by the implementation of an analog filter [5], which is a common component of digital systems. The finite bit and sampling resolution is particularly important for the "fast" signals from scintillator detectors. In order to be recorded with high fidelity, signals from these detectors require subnanosecond sampling frequencies. This enables the digital algorithms to extract information about the signal for the highest relevant frequencies. The availability of gigahertz (GHz) digitizers makes it possible to store signals with subnanosecond accuracy. Unfortunately, these systems suffer from high energy consumption and carry an expensive price-per-channel burden.

Digital timing algorithms extract the time of arrival of a signal from the digitized waveform. Ideally, the timing resolution should only be limited by the detector performance not by the digitizer. This problem can be solved for fast signals using gigahertz digitizers and a digital constant fraction discrimination (DCFD) algorithm [6]. This solution is often difficult or impractical if one is instrumenting a large detector array. As an alternative one could employ slower digitizers (e.g. 100 MS/s) but the timing resolution for these systems may not be adequate for the timing needs.

In experimental nuclear physics, many time-of-flight neutron detectors consist of plastic scintillators, which have signal rise/decay times on the order of a few nanoseconds [7–10]. These detectors rely on analog electronics with conventional CFDs to obtain precise timing. In contrast, nuclear technology applications, e.g. positron emission tomography, use gigasamples-per-second (GS/s) digitizers with fast scintillators, e.g. lutetium orthosilicate (LSO), for timing applications. The time information is extracted using a DCFD or a model is fit to the digitized waveform [11]. These GHz systems are capable of obtaining resolutions on the order of hundreds of picoseconds. Using a

* Corresponding author.

0168-9002/$ - see front matter © 2013 Elsevier B.V. All rights reserved.
http://dx.doi.org/10.1016/j.nima.2013.11.028

40 MS/s digitizer with LSO, Streun et al. perform a linear fit between two points on the leading edge of the waveform to obtain resolutions of 2 ns [12]. These studies demonstrate the necessity of using different algorithms depending on the digitization frequency of the system.

Past work involving digital timing techniques by a University of Florence group applied a 100 MS/s digitizer to signals from a silicon detector [13]. These tests used a digital constant fraction discriminator to achieve timing resolutions on the order of hundreds of picoseconds. Their work demonstrates the necessity for the proper choice of algorithms to determine timing less than the sampling frequency of the digitizers.

To instrument VANDLE, a choice between traditional NIM and digital electronics needed to be made. Digital electronics provided an ideal solution due to previous experience within the group, and their low cost per channel. Ideally, one would instrument VANDLE with GS/s digitizers to minimize the development time necessary to achieve sub-nanosecond time resolution. VANDLE requires many channels of instrumentation and GHz digitizers are still prohibitively expensive. Therefore, we investigated the capabilities of lower frequency systems for the timing applications. This work used XIAs DGF Pixie-16 100 and 250 MS/s digitizers to process the signals from VANDLE.

The challenge is to demonstrate that precise time information can be extracted from the digitized signal when the sampling period is much longer than the characteristic time scale of the signal. While many algorithms exist to accomplish this task, they are not necessarily applicable to every timing situation. The algorithm must take into account the response of the digital system to the raw signal. A Nyquist filter [5] and the sampling frequency of the ADC govern the response. Thus, the problem of timing becomes a deconvolution problem where the major challenge is to determine relevant folding (response) function.

This work tested three numerical algorithms to extract timing information from the digitized signals: a digital constant fraction discriminator (DCFD), a fitting algorithm (FA), and a weighted average algorithm (WAA). To verify these algorithms, a new method to verify the robustness of the digital timing algorithm was developed. The system was tested using an arbitrary waveform generator providing fixed shape pairs of waveforms with various amplitudes and delays. Finally, the digital timing was applied to signals from a plastic scintillator coupled to a photomultiplier tube (PMT). It will be shown that commercially available digital systems, with a low cost per channel, can be used for high resolution timing measurements with fast scintillators.

2. Testing setup and software analysis

This work used an 100 MHz Tektronix AFG3102C Arbitrary Function Generator (AFG) [14]. This function generator allows control of the delay between the signals with 10 ps resolution, their width with 10 ps resolution, and amplitudes with 0.1 mV resolution. A pulse of 10 ns width approximated signals from plastic scintillators. A time calibrator with variable rate triggered the AFG. One volt signals, using half of the ADCs dynamic range, provided a reference signal for the FA. The jitter in the arrival time of signals produced by the AFG is on the order of 50 ps as measured by a 2.5 GS/s oscilloscope. The outputs from the AFG were connected to two adjacent channels in the Pixie-16 digitizers.

The data is read out from the digitizer via a MXI-4 fiber optic crate controller and processed into a data file through a C++ software package. An in-house developed C++ analysis software suite unpacks the data files and processes the raw data stream. A configuration file maps the raw module and channel in the data stream to a specific detector type and performs the appropriate

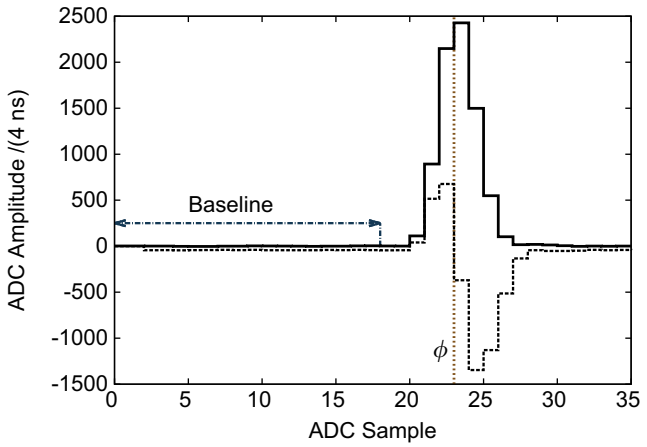

Fig. 1. A sample trace from the 250 MS/s system using the signal produced by the AFG (solid line). The dashed line represents the DCFD for this trace. The position of ϕ is given by the vertical dashed line and is given by zero crossing of the DCFD calculated using Eq. (7) with $D=1$ and $F=0.75$. The horizontal dashed arrow denotes the region used to determine the baseline.

processing. For the work presented here the software applies the timing algorithms to every digitized waveform in the data stream. The average amplitude of all bins up to the signal in the trace constitutes the baseline, denoted by the horizontal dashed arrow in Fig. 1. The standard deviation of the baseline for the AFG is no larger than 1 ADC bin for the cases presented in this work. All of the discussed timing algorithms are implemented in this stage of the analysis and not on-board the digitizer.

3. Digital timing methods

For the Pixie-16 systems used in this work, the digital filter implemented in the FPGA latches and records the digitized waveforms (traces) once a valid trigger is detected. The total trace length and pre-trigger length can both be adjusted by the user. The arrival time of the recorded trace consists of two components. The first component is a 48-bit timestamp, which is the real-time counter value of the FPGA latched at the time of the valid trigger. The time resolution of such a timestamp is obviously limited by the processing clock frequency of the FPGA. The second component is derived from the trace, which is latched with respect to the first component. This position is referred to as the phase (ϕ), and it will be shown that ϕ can be determined to a precision that is smaller than the sampling frequency of the digitizer. The time of a given event in the digitizer is provided by the summation of the filter clock from the FPGA and the phase.

The response of the digital system to a time translation of the raw signal that is below the sampling frequency depends on the derivative of the digitized trace [15]. If the derivative is not constant in the interpolation region, one cannot extract accurate time information using linear methods. If the digitization frequency is substantially faster than the input signal one may assume local linearity. Because the transit times of the scintillators used in this work are much shorter than the digitization period, one can rarely construct a situation where local linearity is achieved. Timing algorithms that do not take into account the non-linear response of the system will not produce accurate results. For these reasons, this work investigated three timing algorithms.

First, the DCFD provides a simple algorithm and was demonstrated to work with digitizers [13,6]. The DCFD applies the following equation to the digitized waveform

$$DCFD[k] = Fy[k] - y[k-D]. \quad (1)$$

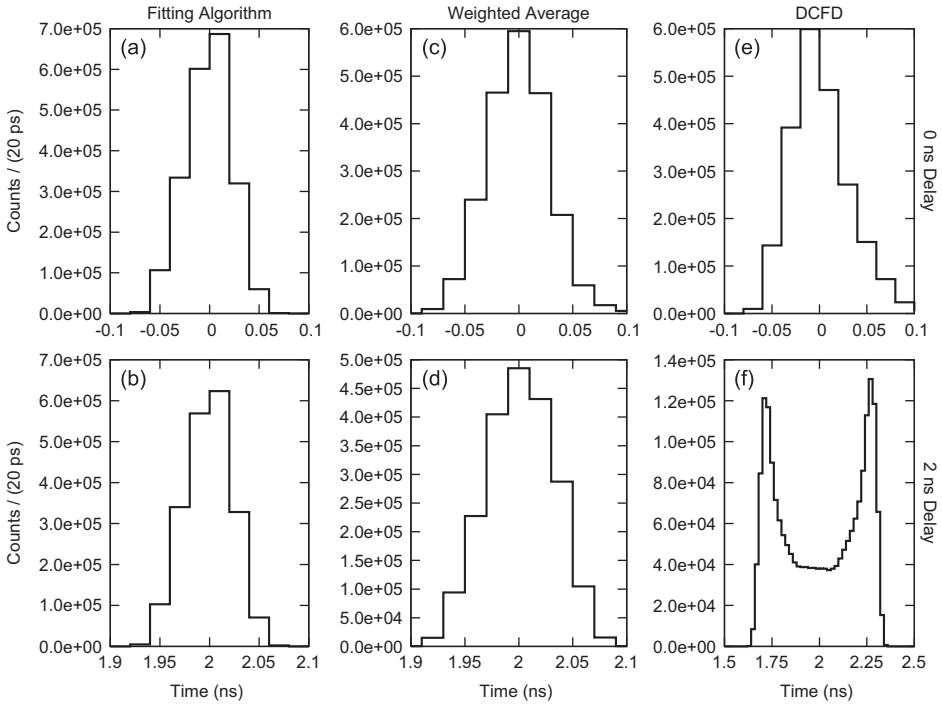

Fig. 2. The resolutions of the various timing methods (columns) for two different signal delays, 0 ns (top row) and 2 ns (bottom row), at a signal amplitude of 1 V. The FA and WAA both produce a well defined peak for both delays. The DCFD fails to reproduce the proper timing when the delay between signals moves to 2 ns.

D is the delay, F is the fraction of the original trace and $y[k]$ is the baseline subtracted amplitude of the trace at bin k [6]. Fig. 1 shows an example of the output of the DCFD algorithm, where $D=1$ and $F=0.75$, for the 250 MS/s system with the associated trace.

The obvious limitation of this algorithm is that the smallest delay available will be equal to the sampling period. To measure subsampling delays, we apply an Akima spline [16] to the data points. Akima splines have a smoother interpolation than a cubic spline, and will produce fewer unnatural spikes in the interpolation. The GNU Scientific Library (GSL) provided the splining algorithms [17]. The spline function increases the number of points available to determine the zero crossing in the hopes of making the behavior of the leading edge of the trace linear in that region. A linear interpolation between points above and below the zero crossing determines its position to better than a sampling cycle.

In a second method, an algorithm fit the digitized waveform. The analytic model approximates the response of the digital system. For this work the function took the following form:

$$f(t) = \alpha e^{-(t-\phi)/\beta}(1-e^{-(t-\phi)^4/\gamma}). \quad (2)$$

The parameter β is the decay constant for the exponential, which is related to the decay of the waveform. The leading edge of the waveform is described by the inverted-squared Gaussian, whose width is given by γ. The normalization of the signal is given by α. The offset ϕ provides the phase of the signal. An averaged waveform fit with all free parameters in Eq. (2) optimizes β and γ. These fitted values are held constant for the timing analysis.

For the pulser signals, the standard deviation of β and γ is 0.01 ns and 0.001 ns^4, respectively. For signals from the detectors described in Section 5, the standard deviation is 0.3 ns and 0.1 ns^4, respectively. Fitting 16 000 traces where all FA parameters are free provides a sample of the possible β and γ values. The sample variance of the set assumes a normal distribution. The square root of sample variance provides the standard deviation of β and γ.

The timing analysis is carried out using a non-linear least squares fitting routine provided by GSL, henceforth referred to as the fitting algorithm (FA). The fitter uses a Levenberg–Marquardt algorithm as implemented in the scaled LMDER routine in MINPACK [17]. The values for β and γ are fixed so that the fitting routine does not fall into nonphysical minima. Should this happen the FA would show a preference for specific values of the phase, which result in inaccurate timing.

The final approach uses the weighted average of the trace. This algorithm will be referred to as the Weighted Average Algorithm (WAA), and the equation is given by

$$\phi = \frac{\sum_{i=\alpha}^{\beta}(y_i-\bar{b})i}{\sum_{j=\alpha}^{\beta}(y_j-\bar{b})}. \quad (3)$$

The parameter y_i is the value of the trace at bin i or j, $\bar{b}$ is the average value of the baseline of the trace (see Fig. 1), α is the starting bin for the weighted average, and β is the final bin for the weighted average. The values for α and β are chosen to optimize the resolution of the system.

Each of the methods described perform timing in the subsampling frequency range. The DCFD and the WAA are possible to implement on-board the digitizers, whereas the FA is much too complicated and requires post processing of the traces. One must take care that the algorithms are behaving as one would expect from the properties of the digital system. To that end, we propose a method that confirms the behavior of the algorithms.

This method relies on the measurement of the time difference between two signals input into the electronics. The first signal has a phase ϕ_1 and the second signal has a phase ϕ_2. The delay (Δ) between the signals is varied in intervals smaller than the sampling frequency of the digitizer to ensure the signals do not sample the same phase space. With a Δ of n times the sampling frequency, a bias of the timing algorithm would be impossible to detect. The measurement of the time difference for the three algorithms is shown in Fig. 2. For a 0 ns delay between the signals (top row), all three of the algorithms produce similar results. This is due to the fact that the delay is equal to an integer multiple of the sampling frequency. Yet, once the Δ moves to 2 ns the DCFD fails to produce a single peak for the time difference indicating

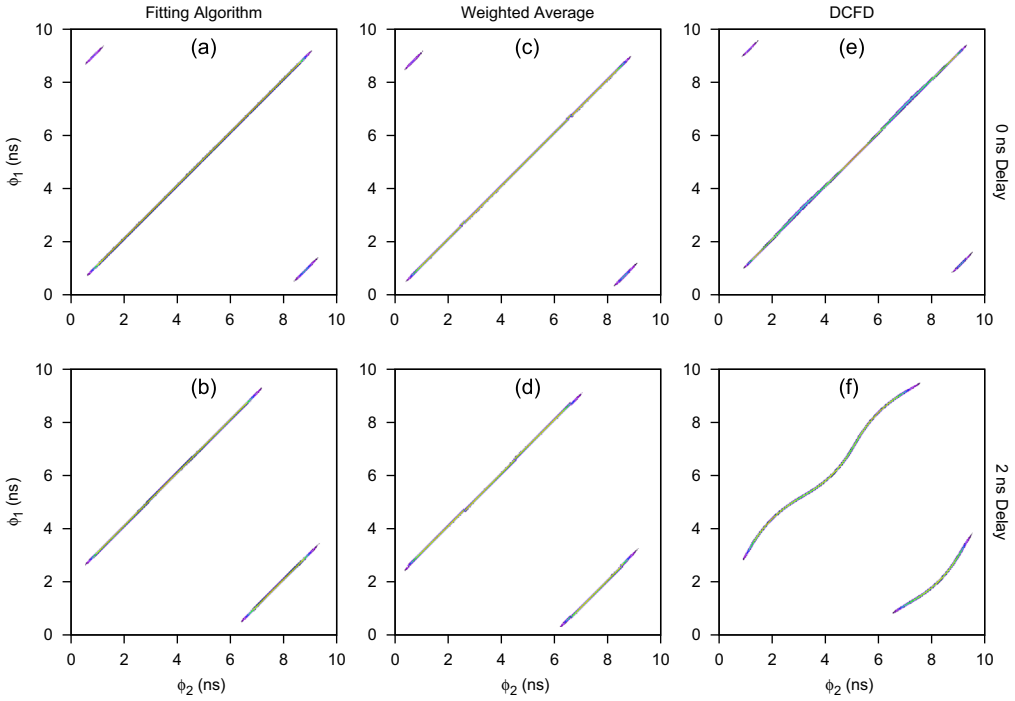

Fig. 3. The phase–phase diagrams of the various timing methods (columns) for two different signal delays, 0 ns (top row) and 2 ns (bottom row), at a signal amplitude of 1 V. The DCFD do not behave according to the strict linear relationship. The small lines appearing at 8 ns from the main distribution are cases where one of the signals has a different timestamp.

that the algorithm is suffering from bias when determining ϕ. The FA and the WAA both produce a single peak for this delay.

The start and stop phases follow a linear relationship given by:

$$\phi_1 = \phi_2 - \Delta, \tag{4}$$

due to the nature of the test setup, and with ϕ_1 random with respect to the sampling clock. A plot of ϕ_1 vs. ϕ_2 immediately indicates the accuracy of the algorithm. A nonlinear relationship reflects deficiencies in the timing algorithm. Fig. 3 displays the phase–phase diagrams for the three timing algorithms (columns). The first row in the figure uses $\Delta = 0$ ns and all of the algorithms display linear results, as one would expect from Fig. 2. The bias of the DCFD becomes rapidly apparent in Panel (f) of Fig. 3, where the strict linear behavior of the system is not maintained. Both the FA and the WAA maintain the linear relationship regardless of the delay between the signals. In each of the graphs, the short lines appearing at 8 ns separation from the main distribution represent cases where the two signals have different filter clock timestamps.

In addition to the linear relationship between phases, one expects that the algorithm does not show bias towards a specific region of the phase space. This would be evidenced by spikes in the distribution of the phase–phase diagrams. Fig. 4(a) shows the projection of the phase–phase diagram for the FA with 2 ns delay (Fig. 3(b)), and Fig. 4(b) is the projection for the DCFD (Fig. 3(f)). One notices immediately the differences between the two methods. The distribution for the FA is flat, as one would expect from the random nature of the start signal, and this result is similar for the WAA. On the other hand, the DCFD shows bias toward specific regions of the phase space. The additional requirement of non-bias in the phase space provides a further confirmation that the algorithm behaves as expected.

The DCFD produces nonlinear results due to the use of a linear interpolation to extract the zero crossing. The derivative of the DCFD waveform determines the accuracy of the DCFD algorithm, and in the studied cases the derivative is nonlinear for fast signals [15]. For these types of signals, the DCFD would produce more accurate results using a faster digitizer, which would achieve local

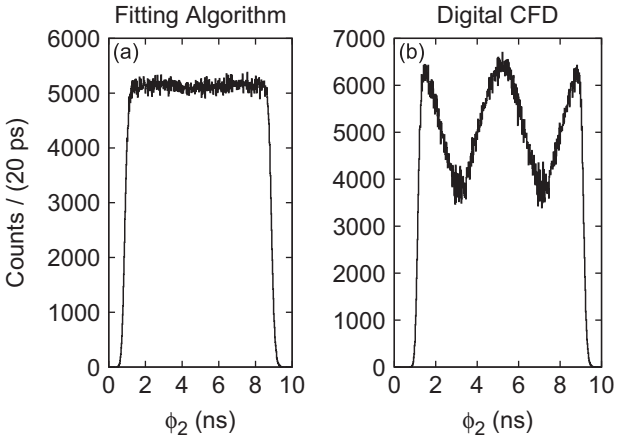

Fig. 4. The projection of the phase–phase diagrams for the FA and the DCFD, each case is for $\Delta = 2$ ns. The FA does not show any bias in the phase space, where as the DCFD is heavily biased because the response of the function is nonlinear in the interpolation region. The WAA produces a projection similar to that of the FA.

linearity around the zero crossing. The FA explicitly takes into account the nonlinear nature of the trace by attempting to reproduce the proper response function for the signal. In the case that one leaves all of the FA parameters free to vary, the results are identical to those of the DCFD due to the highly non-linear nature of the phase sampled by the assumed response function. The FA and WAA, due to the preservation of the linear relationship between the two phases bear further investigation.

4. Performance with an arbitrary function generator

4.1. Setup

The resolution of the two systems (100 MS/s and 250 MS/s) was studied for values of Δ ranging between 0 and 4 ns, and the

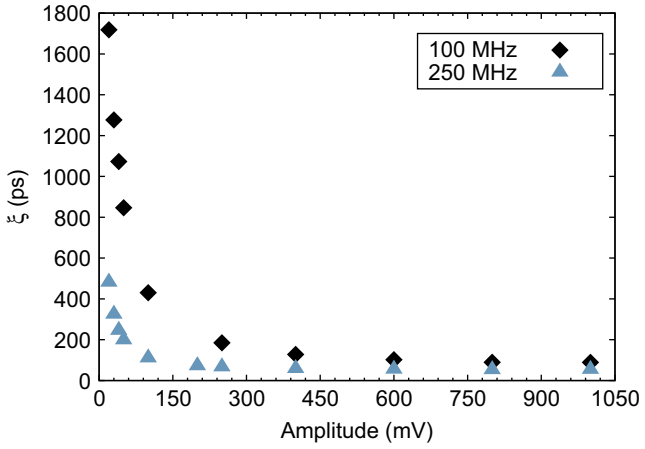

Fig. 5. Time resolution as a function of input voltage for signals from the Tektronix 3102C Arbitrary Function generator using the Fitting Algorithm. The error bars are smaller than the point size.

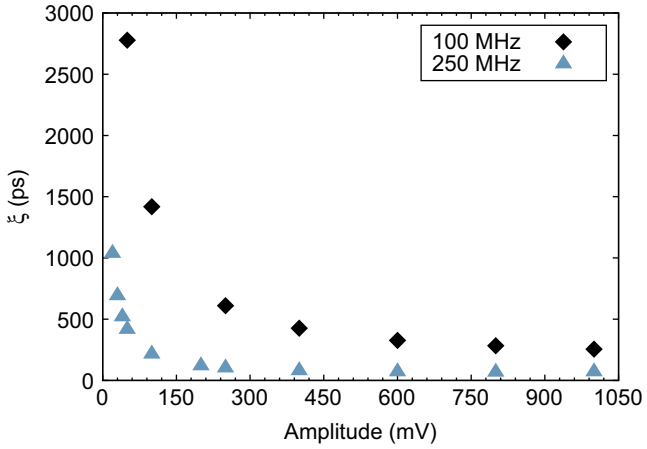

Fig. 6. Time resolution as a function of input voltage for signals from the Tektronix 3102C Arbitrary Function generator using the Weighted Average Algorithm. The error bars are smaller than the point size.

resolution is given by the FWHM of the distributions, seen in Fig. 2 and is denoted by ξ. The sensitivity of the resolution to the amplitude of the input signals was studied in a range of 20 mV to 1 V. The signal-to-noise ratio (SNR) for the 1 V signals was 64 dB for both the systems decreasing to 30 dB for the 20 mV signals.

In all cases, the FA calculated the proper Δ and the phase–phase plots remained linear. The biggest difference between the two systems can be seen in the behavior of the resolution as a function of the amplitude of the input signal. As seen in Fig. 5, the resolution of the 100 MS/s system degrades quickly below 400 mV reaching a value of 1.7 ns for 20 mV signals. For 400 mV and above the 250 MS/s system yields a factor of 2 improvement in the resolution of the system. The largest gain in performance comes for the lowest amplitude signals where a factor of 3.5 is gained.

Similar tests were performed for the WAA for both digitization frequencies. The WAA again maintained the proper phase–phase relationship across all amplitudes and delays. For an optimized choice of averaging window, the WAA performs similarly to the FA. The WAA maintains a resolution of less than the sampling time over the full range, see Fig. 6. Again, the 250 MHz system outperformed the 100 MHz system, leading to a factor of 2.7 improvement at 20 mV.

The WAA while having slightly worse resolution than the FA, 71 ps and 51 ps at 1 V respectively, has an advantage in that it can be relatively easily implemented in a digital system, e.g. on the DSP, which performs floating point operations. This would alleviate the need to store the digitized signals, thus increasing the throughput of the system. In addition, the WAA is more robust than the DCFD when processing fast signals. Due to the poor performance of the WAA for low amplitude signals, a resolution of 1 ns at 20 mV, with the studied systems only the FA is considered for applications to scintillator signals.

5. Application to photomultiplier signals

The application of the FA to a pulser is an idealized situation. To determine the response of the algorithm to a true photomultiplier signal, a pair of test detectors was constructed. The detectors used small $1\times1\times0.4\,\text{in}^3$ pieces of Eljen EJ-200 scintillator coupled to Hamamatsu R580 PMTs from VANDLE. The length of the scintillator crystal contributes approximately 80 ps to the time resolution, given by the transit time of light through the small scintillator chip. The components were arranged into two configurations. The first used a single piece of scintillator material between two PMTs. This detector is optimized for measuring the timing of the system. The second arrangement, optimized for the measurement of timing walk, uses two scintillators each with their own PMT. In each case the scintillator and PMTs were wrapped in a layer of Teflon tape, a layer of Mylar with polymer backing, and black electrical tape.

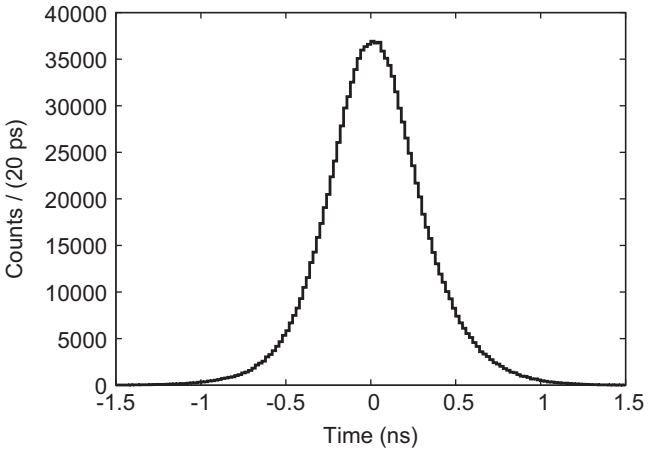

Fig. 7. The time difference between two PMTs in the resolution setup. These signals were analyzed using the Pixie-16-250 setup. The full width at half max is 0.625 ns.

The resulting detectors were connected to the Pixie-16-250 system in the same setup as the pulser. A ^{60}Co source provides a calibration for the PMT. The Compton edge of the source was placed at 75% of the ADCs dynamic range. This means that a majority of the signals will be of high amplitude and as seen in Fig. 5, they will produce the best possible timing. More details of the specific setups follow in the next sections.

5.1. Resolution

The results of the resolution test can be seen in Fig. 7. This resolution is the time difference between the arrival times of the PMTs attached to the small piece of scintillator. The resolution of the system is approximately 0.6 ns over the full range. If only the high energy signals are considered the resolution improves to approximately 0.5 ns. The resolution will be dominated by the transit time of the electrons in the PMTs and not by the algorithm.

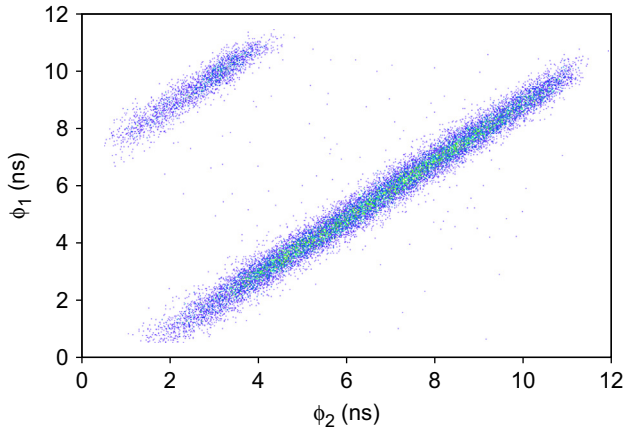

Fig. 8. The phase–phase diagram for the small scintillator detector. The width of the lines is due to the 0.7 ns resolution of the detector. They display the proper linear relationship for timing from the digital system.

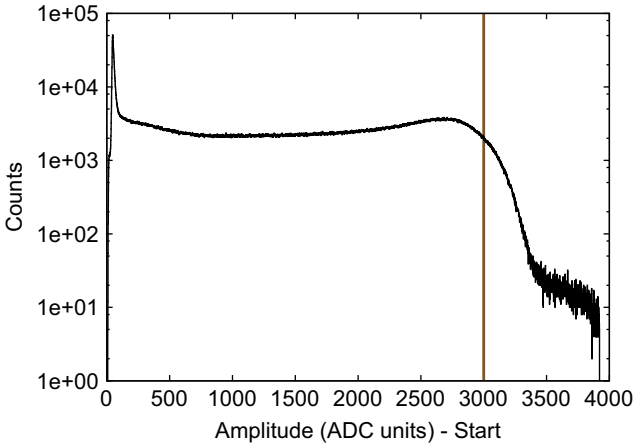

Fig. 9. The amplitude of the start signal. The vertical line represents the software threshold for plotting the Max Amplitude of the stop versus the time difference, Fig. 10.

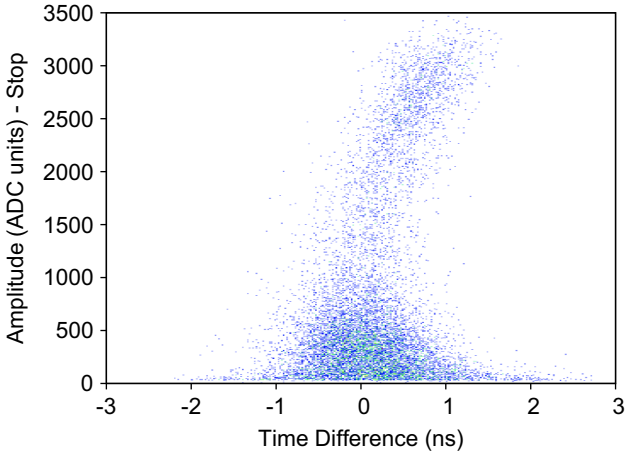

Fig. 10. The amplitude of the stop signal vs. Time Difference for the walk characterization. The start signal is gated on traces that have amplitudes greater than the Compton edge of the source, Fig. 9.

This detector also maintains the linear relationship between the phases, Fig. 8. Both this and the resolution indicate that the FA performs as needed for high resolution timing purposes.

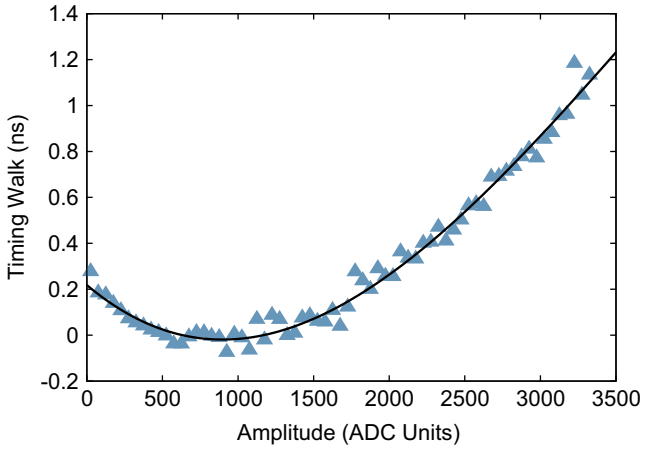

Fig. 11. The timing walk as a function of signal amplitude. The line indicates the fit to the data.

5.2. Timing walk characterization

This measurement used two detectors each consisting of a scintillator coupled to a PMT. The detectors are independently wrapped and timing walk of the system occurs when the relative amplitudes of the signals are mismatched. To measure the timing walk, we use a software gate on signals with amplitude larger than the Compton edge associated with the gamma source, see Fig. 9, and have minimum timing walk. After this condition is imposed the amplitude of the second signal is plot against the time difference between signals, see Fig. 10. Cuts on the amplitude for the second signal are made, which project the time difference. This projection is fit with a Gaussian function, and one can construct a graph of the walk as a function of amplitude, see Fig. 11. A fit applied to these data provides a way to correct the calculated phase.

6. On-board triggering logic

In addition to the digital timing methods, we developed a custom triggering scheme for VANDLE. This triggering scheme allows the system to operate at a low energy threshold while reducing data rates. The triggering scheme, while following standard practices implemented for similar detectors, is unique in that it does not use auxiliary electronics to distribute the implementation across the FPGAs of the data acquisition system. The diagram, Fig. 12, is the schematic representation of the logic gates implemented on the FPGAs. The FPGAs generate the coincidence signals via the on-board logic filters using operating principles developed previously for a segmented germanium detector array [18].

Implementing pairwise coincidences for the PMTs on each VANDLE module provides sensitivity for low energy signals from neutrons, Level 1 in Fig. 12. This operation is implemented locally, as each pair of signals use the same FPGA. The coincidence condition of 100–200 ns reduces the readout rate and is sufficient to nearly eliminate triggers on thermal noise. The pairwise triggering increases the neutron efficiency due to the greatly lowered trigger thresholds, more details on this will be discussed in a subsequent publication [2].

The local coincidence condition is not completely adequate for VANDLEs needs as VANDLE is a time-of-flight detector. This means that VANDLE requires an auxiliary “start” detector, and this start detector must be considered in the full coincidence triggering scheme. The triggers generated by the signals from the start detector are distributed through the backplane bus to all of the

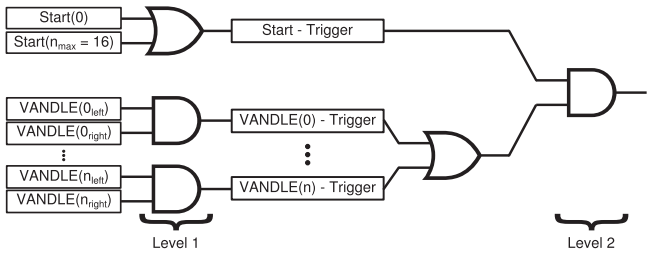

Fig. 12. A schematic of the on-board coincidence triggering used for the VANDLE system. Level 1 indicates the pairwise coincidences between PMTs on a VANDLE module. Level 2 represents the logical AND condition between VANDLE and the start detectors. The system can handle up to 16 start detectors and *n* VANDLE modules.

FPGAs in the system [18]. As is shown in Fig. 12, Level 2 is a logical AND between VANDLE and the start triggers that has a broader time gate, 1 μs long and takes into account the spread in the time of flight. The output of this gate is broadcast back to the trigger bus and seen by all FPGAs and used for validation of the triggers. In this situation the acquisition records only signals that have at least one pair of VANDLE signals and a start detector. The specific detectors producing the start signals vary between experiments: a beta detector for beta-delayed neutron studies or a trigger associated with a specific nuclear reaction. The reliable operation of this coincidence scheme was tested with 3 MHz on the start trigger, which fulfills the requirements for VANDLEs data acquisition. The versatility of the on-board coincidence triggering, as well as the reduced data load, is instrumental to the performance of the digital acquisition system.

7. Conclusions

Three methods for extracting subsampling timing from digitizers were investigated, a digital constant fraction discriminator, a fitting algorithm and a weighted average algorithm. Each of the tested algorithms is capable of subsampling frequency timing. To test the validity of the results from these algorithms a novel technique based upon the properties of the timing structure of the digitizer was developed. This procedure demonstrates that the DCFD does not produce timing information consistent with the known linear behavior of the time structure in the digital system. The FA and the WAA maintain the timing properties of the system.

The time resolution of the FA and the WAA was investigated with an arbitrary function generator. The generator provided two signals with varying delays and amplitudes. The resolution of both algorithms was investigated for both the 100 and 250 MS/s systems. The FA outperformed the WAA over all tested amplitudes, and for both digitizers. The advantage of the WAA is that it is computationally fast and easily implemented on-board in the DSP. Because the FA obtained better resolutions over the full dynamic range of the system it was an ideal candidate to use with fast scintillator detectors.

The timing algorithm was then tested with a small scintillator detector. The timing with this detector proves that the algorithm works well with PMT signals. The resolution of this system was approximately 600 ps for low amplitude signals, which improves to approximately 500 ps for high amplitude signals. These resolutions evince that GHz digitizers are not necessarily required for accurate, precise timing measurements using plastic scintillators.

In addition, an on-board triggering logic provides a method to handle the large amounts of data that are generated when storing the traces for analysis. This triggering scheme is fully implemented on the digitizer and requires no external trigger modules. This is a great advantage when using detector arrays that have a large channel count. As a result of this and the capability of high resolution timing, the Versatile Array of Neutron Detectors at Low Energy has successfully completed a variety of experimental campaigns.

Acknowledgments

The NNSA, through DOE Cooperative Agreement DE-FG52-08NA28552, supported this work.

References

[1] C. Matei, D.W. Bardayan, J.C. Blackmon, J.A. Cizewski, R.K. Grzywacz, S.N. Liddick, W.A. Peters, F. Sarazin, The versatile array of neutron detectors at low energy (VANDLE), in: Proceedings of the Ninth International Symposium on Nuclei in the Cosmos, vol. 138, Proceedings of Science, 2008, pp. 1–5.
[2] W.A. Peters, R. Grzywacz, J.A. Cizewski, M. Madurga, S.V. Paulauskas, S. Ilyushkin, F. Sarazin, J. Blackmon, C. Matei, I. Spassova, the VANDLE Collaboration, Performance of the Versatile Array of Neutron Detectors at Low Energy (VANDLE), in preparation for publication in NIMA, 2014.
[3] S. Mitra, L. Wielopolski, G. Hendrey, Appl. Radiat. Isot. 61 (6) (2004) 1463 http://dx.doi.org/10.1016/j.apradiso.2004.02.024. URL ⟨http://www.sciencedirect.com/science/article/pii/S0969804304001514⟩.
[4] A. Al-Adili, F.-J. Hambsch, S. Oberstedt, S. Pomp, S. Zeynalov, Nucl. Instrum. Methods Phys. Res. Sect. A Acceler. Spectrometers Detectors Assoc. Equip. 624 (3) (2010) 684 http://dx.doi.org/10.1016/j.nima.2010.09.126. URL ⟨http://www.sciencedirect.com/science/article/pii/S0168900210021595 ⟩.
[5] H. Nyquist, Trans. Am. Inst. Electr. Eng. 47 (1928) 617.
[6] A. Fallu-Labruyere, H. Tan, W. Henning, W.K. Warburton, Nucl. Instrum. Methods Phys. Res. Sect. A 579 (2007) 247.
[7] T. Blaich, T. Elze, H. Emling, H. Freiesleben, K. Grimm, W. Henning, R. Holzmann, G. Ickert, J. Keller, H. Klingler, W. Kneissl, R. König, R. Kulessa, J. Kratz, D. Lambrecht, J. Lange, Y. Leifels, E. Lubkiewicz, M. Proft, W. Prokopowicz, C. Schütter, R. Schmidt, H. Spies, K. Stelzer, J. Stroth, W. Walus, E. Wajda, H. Wollersheim, M. Zinser, E. Zude, Nucl. Instrum. Methods Phys. Res. Sect. A 314 (1) (1992) 136, http://dx.doi.org/10.1016/0168-9002(92)90507-Z.
[8] A. Buţă, T. Martin, C. Timiş, N. Achouri, J.C. Angélique, C. Borecea, I. Cruceru, A. Genoux-Lubain, S. Grévy, M. Lewitowicz, E. Liénard, F.M. Marqués, F. Negoiţă, F. de Oliveria, N.A. Orr, J. Péter, M. Sandu, Nucl. Instrum. Methods Phys. Res. Sect. A 455 (2000) 412.
[9] B. Luther, T. Baumann, M. Thoennessen, J. Brown, P. DeYoung, J. Finck, J. Hinnefeld, R. Howes, K. Kemper, P. Pancella, G. Peaslee, W. Rogers, S. Tabor, Nucl. Instrum. Methods Phys. Res. Sect. A 505 (2003) 33.
[10] G. Perdikakis, M. Sasano, S.M. Austin, D. Bazin, C. Caesar, S. Cannon, J. Deaven, H. Doster, C. Guess, G. Hitt, J. Marks, R. Meharchand, D. Nguyen, D. Peterman, A. Prinke, M. Scott, Y. Shimbara, K. Thorne, L. Valdez, R. Zegers, Nucl. Instrum. Methods Phys. Res. Sect. A 686 (0) (2012) 117, http://dx.doi.org/10.1016/j.nima.2012.05.076, URL ⟨http://www.sciencedirect.com/science/article/pii/S0168900212005906 ⟩.
[11] M. Aykac, I. Hong, S. Cho, Nucl. Instrum. Methods Phys. Res. Sect. A 623 (2010) 1070.
[12] M. Streun, G. Brandenburg, H. Larue, E. Zimmermann, K. Ziemons, H. Halling, Nucl. Instrum. Methods Phys. Res. Sect. A 487 (2002) 530.
[13] L. Bardelli, G. Poggi, M. Bini, G. Pasquali, N. Taccetti, Nucl. Instrum. Methods Phys. Res. Sect. A 521 (2004) 480.
[14] Tektronix, Arbitrary Function Generators: AFG3000C Series. URL ⟨http://www.tek.com/signal-generator/afg3000-function-generator ⟩.
[15] M. Madurga, S.V. Paulauskas, R. Grzywacz, S.W. Padgett, D.W. Bardayan, J. C. Batchelder, J.C. Blackmon, J.A. Cizewski, R.E. Goans, S.N. Liddick, P. O'Malley, C. Matei, W.A. Peters, C. Rasco, F. Raiola, AIP Conf. Proc. 1336 (1) (2011) 586, http://dx.doi.org/10.1063/1.3586170, URL ⟨http://link.aip.org/link/?APC/1336/586/1⟩.
[16] H. Akima, J. Assoc. Comput. Mach. 17 (4) (1970) 589.
[17] M. Galassi, J. Davies, J. Theiler, B. Gough, G. Jungman, P. Alken, M. Booth, F. Rossi, GNU Scientific Library Reference Manual, Network Theory Ltd., 2009, accessed on line; 10 January 2013. URL ⟨https://www.gnu.org/software/gsl/manual/html_node/⟩.
[18] K. Starosta, C. Vaman, D. Miller, P. Voss, D. Bazin, T. Glasmacher, H. Crawford, P. Mantica, H. Tan, W. Hennig, M. Walby, A. Fallu-Labruyere, J. Harris, D. Breus, P. Grudberg, W. Warburton, Nucl. Instrum. Methods Phys. Res. Sect. A Accel. Spectrometers Detectors Assoc. Equip. 610 (3) (2009) 700, http://dx.doi.org/10.1016/j.nima.2009.09.016, URL ⟨http://www.sciencedirect.com/science/article/pii/S0168900209017392⟩.